A KALMAN-BASED IDENTIFICATION APPROACH FOR DISTRIBUTED AERODYNAMIC LOADS ON A ROTATING BLADE

Roberta Cumbo [1,2], Tommaso Tamarozzi [1,2], Wim Desmet [2,3], Pierangelo Masarati [4]

[1] Siemens Digital Industries Software, Interleuvenlaan 68, 3001 Leuven, Belgium
[2] Katholieke Universiteit Leuven, Celestijnenlaan 300 B, 3001 Heverlee, Belgium
[3] DMMS-D core lab, Flanders Make, Belgium
[4] Politecnico di Milano, Via Giuseppe La Masa 34, 20156 Milano, Italy

Abstract
The rotating blades of the helicopter are constantly interacting with the external fluid generating vibratory loads. These excitations are then transmitted to the rotor hub and can lead to failures in the main rotor system. The knowledge or prediction of the aerodynamic loads become thus of great importance for design and failure prevention. Several experiment-based and model-based techniques have been presented in literature, but given the complexity in helicopter modelling, high accuracy can only be reached if a large amount of sensor data and/or a high-fidelity numerical model is available. This contribution focuses on the usage of the Kalman filtering technique for rotor load estimation. The filter presents two main advantages: i) usage of a minimum set of sensors; ii) compensation of a low-fidelity model by accounting for sensor and model uncertainties. The problem of state and load estimation is addressed in this paper on a rotating helicopter blade through a numerical example. Numerical results show an accurate state reconstruction with respect to the selected sensor layout and model uncertainties. The distributed aerodynamic loads can be accurately reconstructed in post-processing.

1. INTRODUCTION

The mechanical components of a helicopter rotor are continuously subject to time-varying loads, which are generated by highly flexible rotating blades interacting with the aerodynamic flow and transmitted to the rotor hub. These loads heavily affect the life of the rotor's components and thus of the entire structure. The knowledge of the aerodynamic and inertia loads acting on the blades becomes then of significant importance, since they are potential sources of failure in operating conditions. Several approaches combining test and model solutions [1-9] have been exploited in literature to predict/estimate the dynamic behavior of the blades. Among these techniques, the so-called blade shape sensing [8-9] has been demonstrated to be an efficient modal-based approach to reconstruct the shape of the blade combining a limited set of measurements with the modal shapes. If an accurate knowledge of the model is not available, another alternative is the usage of estimators. The Kalman Filter [10-11] is an efficient technique to address the problem of state and load reconstruction. This methodology aims to solve a state space model taking into account the statistics of the model and measurement uncertainties. The filter operates in two main phases, identified as prediction and correction. The model predicts the state in the next time instant. This prediction is then corrected through the update equations of the filter, using the measurement data given as input to the algorithm at each time step. This principle is schematically shown in Fig. 1.

Figure 1. Prediction-correction structure of the Kalman Filter.

There are several variants of the Kalman Filter in literature [12-18]. The most suitable for input estimation in terms of efficiency and computational costs is the Augmented Kalman Filter, which has recently been succesfully applied to automotive applications [19-20].

This contribution aims to show the effectiveness and robustness of the Augmented Kalman Filter (AKF) on helicopter blade models. The presented study makes use of a simplified multi-body [21] model, shown in [22], of an articulated 2-blade rotor, validated with simulation data obtained through MBDyn [23]. The focus is on the hovering flight-condition and the Blade Element Momentum Theory (BEMT) [24] is applied for the aerodynamic evaluation on the discretized blade, i.e. defined by rigid bodies

Presented at 46th European Rotorcraft Forum, Moscow, Russia, 8-11 September, 2020

connected by elastic elements [25]. In the case of a not highly validated model, the results in previous works [19-20] show the good estimation of the states with loss of accuracy in the load estimation. This is due to the fact that all the missing physics information in the model is compensated in the loads. In the specific case of helicopter blades, the aerodynamic loads are functions of the aerodynamic coefficients, the inflow velocity and the states of the blade, i.e. pitch angle and velocity.

The proposed approach aims to use a reduced set of sensors along the blade, needed to obtain the prediction of the full-field response with high accuracy. The second step concerns the extrapolation of predicted responses along the blade span. These quantities will be used then to evaluate the distributed aerodynamic loads, i.e. drag and lift. In this contribution, the robustness of the proposed method is demonstrated on simulated data through a numerical example in which the source of uncertainties is in the model parameters.

2. DISCRETE-TIME AUGMENTED KALMAN FILTER

The Kalman Filter is an optimal estimator which operates in a state-space formulation. Given *x* states of the system and *y* observations, a time-discrete first-order model at the time-step *k* can be expressed as:

$$(1)\quad \begin{cases} x_{k+1} = Ax_k + Bp_k + w_{x,k} \\ y_{k+1} = Cx_{k+1} + Dp_{k+1} + w_{y,k+1} \end{cases}$$

where *A, B* are time-invariant matrices depending on the system dynamics, *C, D* depend instead on the nature of the observations. w_x and w_y are respectively the zero-mean Gaussian model and measurements noise. In the augmented formulation, the input vector *p* is an unknown variable and an augmented state vector is introduced as:

$$(2)\quad x_{a,k} = [x_k,\ p_k]^T$$

By plugging Eq. (2) into Eq. (1) and using a zero-th order input model, i.e. $p_{k+1} = p_k + w_p$, it is possible to obtain the following system:

$$(3)\quad \begin{cases} x_{a_{k+1}} = Ax_{a_k} + w_{x_a,k} \\ y_{k+1} = Hx_{a_{k+1}} + w_{y,k+1} \end{cases}$$

where *H* is the augmented observation matrix, i.e. $H = [C,\ D]$, and w_{x_a} is the Gaussian noise which includes model and input uncertainties. The step from continuous-time to discrete-time formulation is not straightforward. Indeed, the application of Eq. (1) or (2) depends on the discretization scheme adopted in the model. Further details related to the adopted multibody model will be given in the next section. Important features and tuning parameters of the Kalman Filter are the covariance matrices *Q* and *R* associated respectively to w_{x_a} and w_y. The matrix Q is block-diagonal and usually, the only non-null sub-block is the one related to the input model, which is the main source of uncertainties.

The Kalman Filter is executed in two main steps:

1. Prediction: integration of the equation of motion at the time-step *k,* with zero-noise.
2. Correction: updating of the predicted states $x_{a\,k+1}^-$ with the available observations *y* at time-step *k+1:*

$$(4)\quad x_{a\,k+1}^+ = x_{a\,k+1}^- + K_{k+1}(y_{k+1} - Hx_{a\,k+1}^-)$$

In Eq. (4), *K* indicates the optimal Kalman gain, which is evaluated by means of the minimization of the state-covariance matrix *P.*

In the framework of augmented filtering, the number and type of sensors is important in order to reach a stable estimation. As demonstrated in [26], a number of position-level sensors equal or greater than the number of input loads to be estimated are needed.

3. MULTIBODY MODEL OF A ROTATING BLADE

In this paper, the blade multibody model shown in [22] is considered and it will be briefly described in this section.

A multibody simulation can be carried out on i) ordinary differential equations (ODE), ii) differential-algebraic equations (DAE). When the problem is stiff, i.e. with the presence of solutions varying slow and varying rapidly, the DAE formulation is most suitable [27]. If an ODE formulation is considered, numerical instabilities might occur, unless the integration time-step is extremely small. An index-2 DAE Gear Gupta Leimkuhler (GGL) [28] approach is thus chosen, which formulates the continuous-time equation of motion of a constrained system as follows:

$$(5)\quad \begin{cases} \dot{q}(t) - v(t) + B\big(q(t)\big)^T \mu_S(t) = 0 \\ M\big(q(t)\big)\dot{v}(t) + f\big(q(t), v(t)\big) - B\big(q(t)\big)^T \lambda_s = 0 \\ B\big(q(t)\big)^T v(t) = 0 \\ g\big(q(t)\big) = 0 \end{cases}$$

In Eq. (5): *q* and *v* are the coordinate and velocity vectors of the system; $\dot{q}$ and $\dot{v}$ are the time derivatives of *q* and *v; M* is the mass matrix; *f* is a general non-linear term including all elastic, external and quadratic forces; *B* is the Jacobian matrix of the constraints; λ_s and μ_s are respectively the Lagrange multipliers and the velocity-level multipliers; *g* is the

Presented at 46th European Rotorcraft Forum, Moscow, Russia, 8-11 September, 2020

set of algebraic equations which includes all the geometric relations.

The blade in [22] is discretized as composed by N_b rigid bodies and $(N_b - 1)$ flexible elements. A Finite Segment Beam approach is adopted as described in [29]. The flexible elements are modelled as 6 Degrees of Freedom (DoFs) spring. Given two bodies as in Fig. (2), the elastic interaction is quantified with the equivalent stiffness evaluated as a series of springs:

(6) $k_{12} = \frac{k_{1b}k_{2a}}{k_{1b}+k_{2a}}$

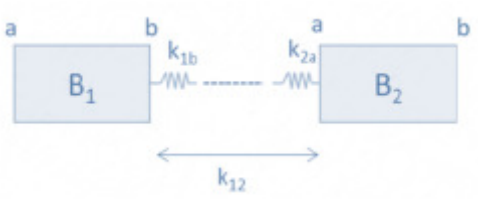

Figure 2. Scheme of two rigid bodies connected with elastic elements.

Each spring is characterized by an elemental stiffness matrix k_{if}.

3.1. Kalman Filter estimation

As stated in Sec. (2), the application of the Kalman Filter on a discrete-time model of this complexity is not straightforward and it needs an additional step, which is the discretization of the continuous-time model. The multibody solver used in the present work computes this step by applying the implicit Backward Differentiation Formulas (BDF) integration method [31]:

(7) $\dot{z}_{k+1} = \sum_{j=0}^{s} \alpha_j z_{k+j}$

with s and α as order and coefficients of the adopted BDF scheme, and z as a general variable with time derivative $\dot{z}$. A first order integrator has been used in this contribution. As example, the first order integration of the state vector $\dot{x}$ is:

(8) $\dot{x}_{k+1} = \alpha(x_{k+1} - x_k)$

By looking at the GGL formulation in Eq. (5), the state vector can be defined as:

(9) $x = [q, v, \lambda_s, \mu_s]^T$

If an augmented estimation will be executed, the following augmented state vector needs also to be defined:

(10) $x_a = [x^T, p]^T$

Eq. (7) allows to compute the first order time-derivatives of the augmented state vector. At this stage, the discrete-time scheme of the GGL problem can be defined and it will represent the numerical model on which the Augmented Kalman Filter will be applied:

$$(11)\quad \begin{cases} \dot{q}_{k+1} - v_{k+1} + B(q_{k+1})^T \mu_{s,k+1} = 0 \\ M(q_{k+1})\dot{v}_{k+1} + f(q_{k+1}, v_{k+1}, p_{k+1}) - B(q_{k+1})^T \lambda_{s,k+1} = 0 \\ \dot{p}_{k+1} = 0 \\ B(q_{k+1})^T v_{k+1} = 0 \\ g(q_{k+1}) = 0 \end{cases}$$

In Eq. (11), the zero-th order random walk model of the input ***p*** is added to the set of equations of motion. Note also that the dependence of the force vector ***f*** from the variable ***p*** is explicitly reported.

4. AERODYNAMIC MODEL

A 2D aerodynamic model is employed in the present work and the inflow velocity is evaluated as formulated in the Beam Element Momentum Theory (BEMT) [24].

Given the Fig. (3), the elemental lift and drag at the section ***r*** is expressed as:

(12) $dL = \frac{1}{2}\rho\, \dot{q}^T\, \dot{q} C_L c\, dr$

$dD = \frac{1}{2}\rho\, \dot{q}^T\, \dot{q} C_D c\, dr$

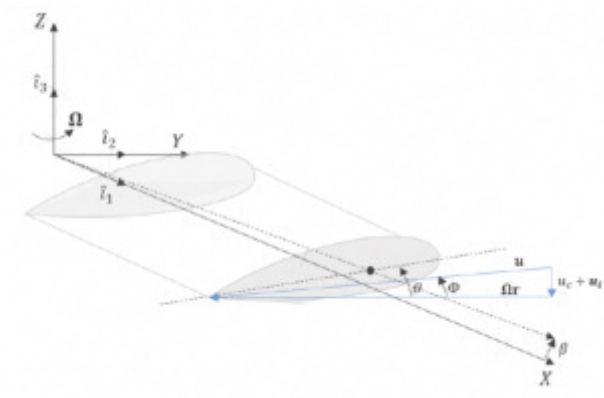

Figure 3. Airfoil scheme at a given blade section.

The airfoil associated to this model is a symmetric NACA0012 profile and for this reason, no aerodynamic pitch torque is considered.

In Eq. (12): ρ is the air density, $\dot{q}$ is the velocity of the rigid body at the stage ***r***, $\dot{\beta}$ is the flapping velocity, ***c*** is the chord of the blade at the stage ***r***.

C_L and C_D are the aerodynamic coefficients. In general, they are tabular values for a given airfoil. Important for the evaluation of the total thrust

Presented at 46th European Rotorcraft Forum, Moscow, Russia, 8-11 September, 2020

produced by the rotating blades is the expression of the lift coefficient C_L. This contribution focuses on small angles of attack α and low values of the Mach number, such that a linear relation $C_L = a\alpha$ is guaranteed, with *a* representing the lift slope of the section, and the angle of attack $\alpha = \theta - \Phi$. θ and Φ are respectively the pitch and inflow angles of the section.

The velocity vector of a point that resides on an axis parallel to $\hat{\imath}_1$ can be expressed as:

(13) $\dot{q} = \Omega\,\hat{\imath}_3 \times \boldsymbol{r} + \dot{\beta}|\boldsymbol{r}|\hat{\imath}_3 + (u_1\hat{\imath}_1 + u_2\hat{\imath}_2 + u_3\,\hat{\imath}_3)$

where Ω is the rotational speed and $\hat{\imath}_1, \hat{\imath}_2, \hat{\imath}_3$ are the unit-vectors rotating with the rotor hub. In the vertical component of the velocity, the contribution of the inflow velocity u_i is included. This effect is given by the volume of air that is moved by the rotor. In this contribution, a uniform inflow model is considered and it is briefly discussed in the following.

4.1. Uniform Inflow Model

A uniform inflow model based on the BEMT theory is used, which is an acceptable approximation for hovering or in general in quasi-steady flight conditions. The inflow velocity can be written as:

(14) $u_i = \sqrt{\frac{T}{2\rho A}}$

with *T* total thrust produced by the rotor disk and *A* rotor disk area. In the following, we will refer to the induced velocity as its dimensionless value

(15) $\lambda_i = \frac{u_i}{\Omega R}$

with *R* as radius of the blade. The sectional inflow angle becomes:

(16) $\Phi = \frac{u_i}{\Omega r} = \frac{\lambda_i}{x}$

with $x = r/R$, i.e. dimensionless spanwise position of the blade section. The value of the induced velocity is constantly updated depending on the value of the thrust produced by the rotor disk, which takes the form:

(17) $T = \frac{1}{2}\rho a b \Omega^2 \int_0^R c(\theta - \Phi) r^2 dr$

From the Eq. (16) and Eq. (17), an implicit problem needs to be solved iteratively. A Newton-Raphson method [31] is adopted in this work as in [22]. The following implicit function is defined:

(18) $f(\lambda) = \lambda - \frac{C_T(\lambda)}{2\sqrt{\mu^2+\lambda^2}} = 0$

with μ as dimensionless air velocity parallel to the rotor disk, i.e. $\mu = \frac{|u|\cos\alpha}{\Omega r}$, and $\lambda = \mu\tan(\alpha) - \lambda_i$. C_T is the blade loading coefficient or dimensionless thrust, i.e. $C_T = \frac{T}{\rho A(\Omega R)^2}$. For small values of μ, the hovering value of the induced velocity can be used as first guess of the iterative process, i.e. $\lambda_0 = \sqrt{\frac{C_T}{2}}$.

5. NUMERICAL 2-BLADE ROTOR MODEL

The model presented in this section is the one developed in [22]. It is an articulated rotor with two blades. Each blade is modelled as composed by four rigid bodies, connected through elastic elements. In Table (1), all the physical features are listed. The elastic properties are reported according with the finite element beam theory [32].

Blade Structural Properties			Blade Elastic Properties		
Total mass	82.76	kg	EA	5.69E8	N
Chord	0.537	m	EI_{yy}	4.00E5	Nm^2
Total Length	6.988	m	EI_{zz}	4.00E5	Nm^2
Radius	7.420	m	GJ	8.40E5	Nm^2/rad

Root hinges – distance from Hub			Root hinges – elastic properties		
Flap offset	0.289	m	Flap damping characteristic	7.50E3	Nms/rad
Lag offset	0.269	m	Lag damping characteristic	7.50E3	Nms/rad
Pitch offset	0.432	m			

Table 1. Blade and rotor features.

The simulated flight condition has rotational speed $\Omega = 60\text{RPM}$ and pitch angle $\theta = 3deg$. The aerodynamic profile is the symmetric NACA0012. Gravity has been also applied and the rotor is fixed to the ground. The scheme of one single blade is shown in Fig. (4): the aerodynamic forces are applied at each rigid body in the aerodynamic centre, i.e. quarter chord for symmetric profile.

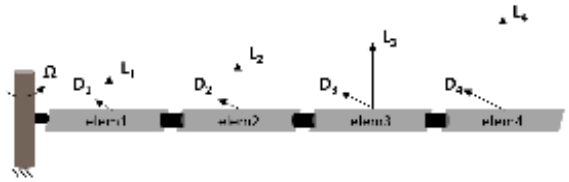

Figure 4. Single blade discretized with 4 elements.

5.1. User model vs Reference model

In this contribution, the performance of the Augmented Kalman Filter for joint input and states estimation is shown on a numerical example and the presented source of uncertainties is in the model. We will refer to *user model* as the model on which the

Presented at 46th European Rotorcraft Forum, Moscow, Russia, 8-11 September, 2020

filter operates and to *reference model* as the model from which the reference measurements are selected. In order to quantify how much the filter can mitigate the presence of uncertainties, the two models should differ such that some modelling errors can be considered.
The reference model has been developed in MBDyn [23], in which the blade model is discretized according with the finite volume formulation [33]. The flexible element connects three nodes, i.e. bodies, and the internal forces are evaluated in well-chosen points between the two endpoints. In the Finite Segment Formulation, the flexible element connects instead two bodies. The different modelling is thus in the internal forces evaluation and even in the mass distribution along the blade. A sketch of the two approaches for one flexible element of free-length *l* is shown in Fig. (5).

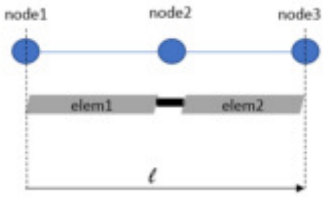

Figure 5. Sketch of flexible element modelling according with Finite Volume (nodes) and Finite Segment (elem) formulations.

In the user model the number of rigid bodies N_b and flexible elements N_f are $N_b = 4$, $N_f = 3$; while in the reference model $N_b = 5$, $N_f = 3$.

In Fig. (6) and (7), the vertical displacements reached in steady state and the relative percentage error along the span of the blade is shown for the 2-blade rotor in rotation and under gravity (gradually applied). In Fig. (8) and (9), the same comparison is shown but also aerodynamic loads are applied.

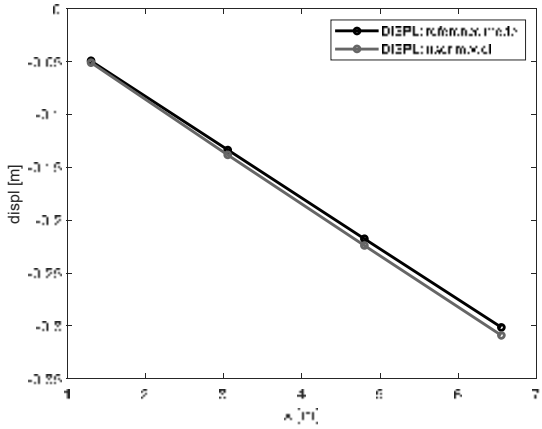

Figure 6. Rotating blades under gravity. Vertical displacement distribution along the span, in steady condition. Blade in rotation and under gravity.

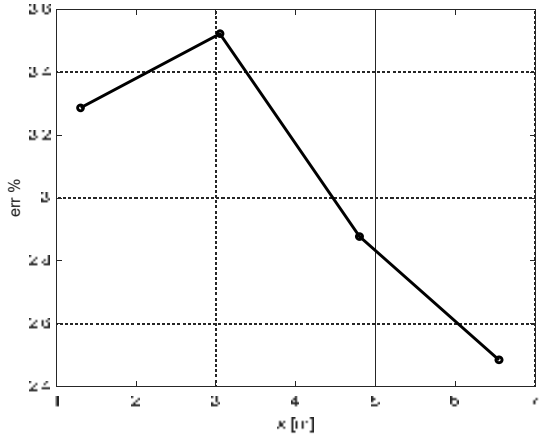

Figure 7. Rotating blades under gravity. Relative percentage error between displacement fields of Fig. 6 (reference and user model solutions).

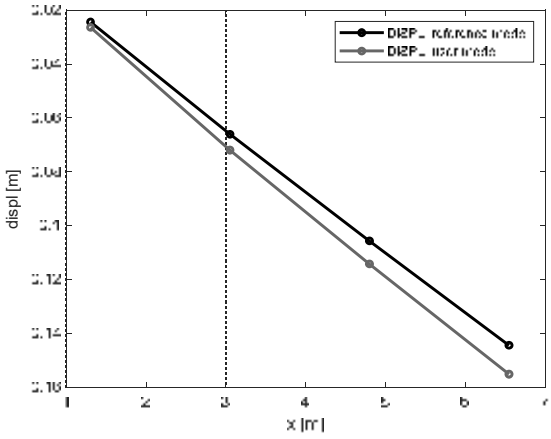

Figure 8. Rotating blades under gravity. Aerodynamics applied. Vertical displacement distribution along the span, in steady condition. Blade in rotation and under gravity.

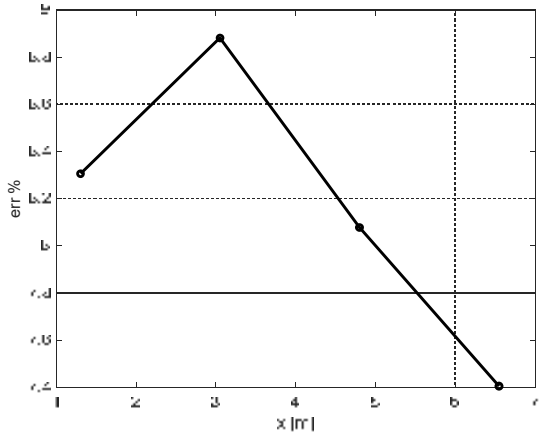

Figure 9. Rotating blades under gravity. Aerodynamics applied. Relative percentage error between displacement fields of Fig. 6 (reference and user model solutions).

Presented at 46th European Rotorcraft Forum, Moscow, Russia, 8-11 September, 2020

5.2. Augmented Kalman Filter estimation

The sensors' layout used in the proposed numerical estimation is listed in Table (2) with reference to the elements in Fig. (4). *x, y, z* are the directions in the fixed reference frame. The sensors were located on *elem3* and *elem4* because they are more sensitive to the applied loads. The velocity sensors allow also to capture the flapping motion.

Position sensors		Velocity sensors	
elem3	z	elem3	z
elem4	z	elem4	z

Table 2. First sensors layout.

The estimation is performed by simulating the model without embedded aerodynamics. The aerodynamic forces are instead considered as external and unknown. Given the higher contribution that the lift produces on *elem3* and *elem4,* only the corresponding lift forces will be estimated. All the other aerodynamic forces will be not considered in the estimation. As explained in [22], this assumption is made because of two main reasons:

1. Reduced number of sensors needed;
2. The aerodynamic loads can be estimated a-posteriori if the knowledge of the full displacement and velocity field is correctly reconstructed.

The results of the estimation in terms of displacement field is shown in Fig. (10) as relative percentage error. Looking at Fig. (9), a great improvement of the error on the displacement field can be observed with respect to simulated data.

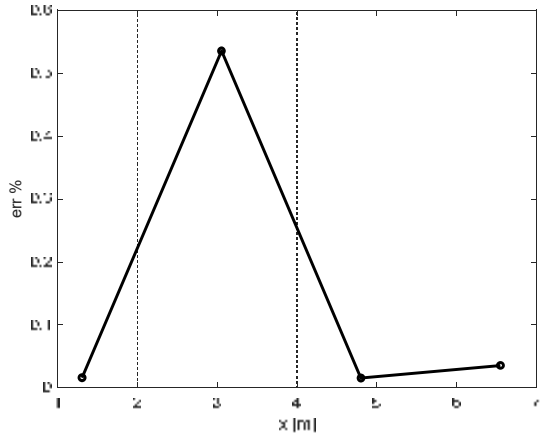

Figure 10. Rotating blades under gravity. Relative percentage error between displacement field of reference model and the estimated one by using the sensors layout in Table 2.

In Fig. (11), the estimation of the sensors data included in the filter is shown and a good matching can be observed. Fig. (12) shows instead a different conclusion: the filter cannot compensate for both modelling and force errors and this is observed on the velocities in the *y* (in-plane) direction. Theoretically, these quantities should be the same in the two models, because the in-plane velocity is almost equal to Ωr for each position r along the blade span. The sensors layout in Table (2) cannot guarantee the observability of the in-plane motion. In order to improve the accuracy of the results, a different sensors layout is proposed and listed in Table (3).

Position sensors		Velocity sensors	
elem3	z	elem3	z
elem4	z	elem4	z
elem4	y		

Table 3. Second sensors layout.

The improvement can be observed in Fig. (13), which shows that the delay obtained through the first sensors layout is now compensated.

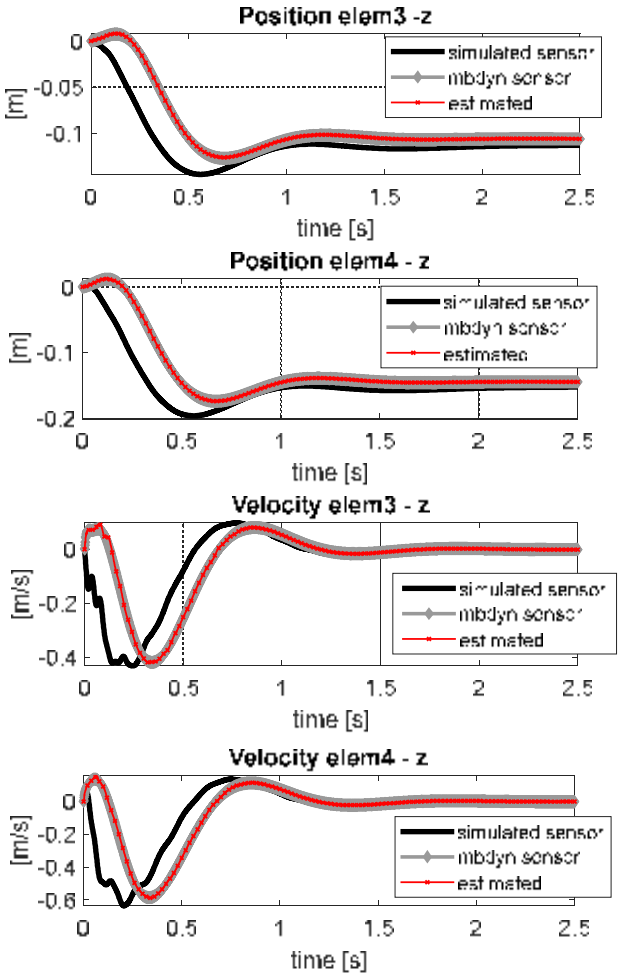

Figure 11. Estimation of sensors data. Sensors layout in Table (2).

Presented at 46th European Rotorcraft Forum, Moscow, Russia, 8-11 September, 2020

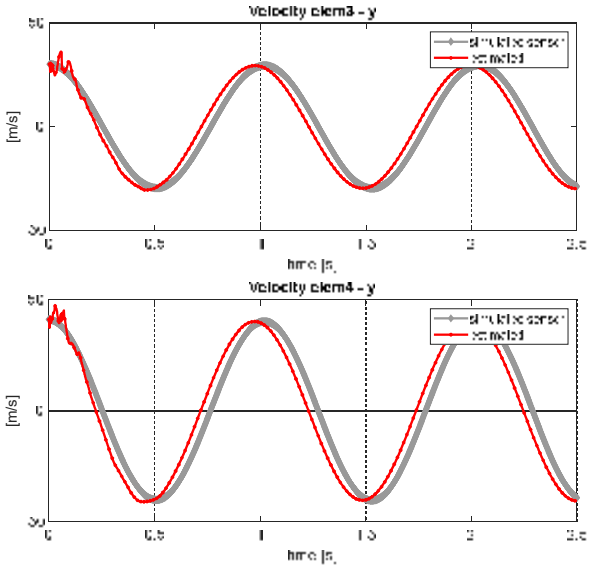

Figure 12. Estimated velocity states of element 3 and 4 in y-direction. Sensors layout in Table (2).

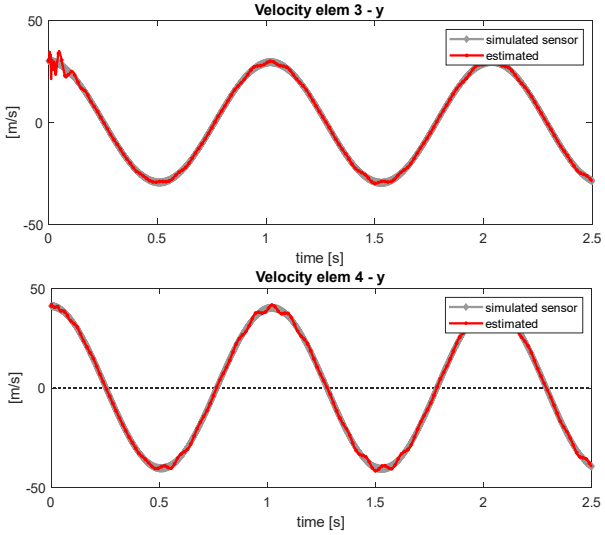

Figure 13. Estimated velocity states of element 3 and 4 in y-direction. Sensors layout in Table (3).

5.3. Load estimation

As example, the estimation of the external (aerodynamic) loads acting on *elem3* and *elem4* are shown in Fig. (14) for the first sensors layout in Table (2) and compared with the reference values from MBDyn. The modelling errors assumed in the estimation are compensated by the filter in the estimated loads and thus the values are quite off.

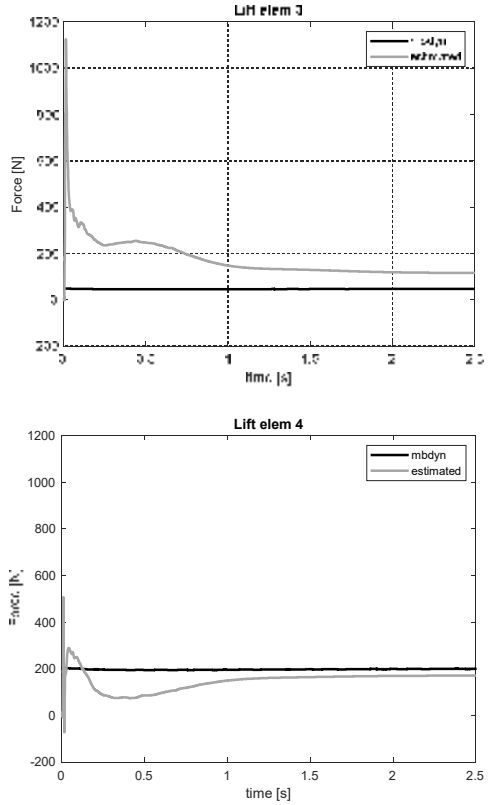

Figure 14. Lift estimation on elem3 and elem4. Comparison with reference data from MBDyn.

In [22], an improvement of the loads estimation is proposed by reconstructing the aerodynamic loads in post-processing, leveraging from the knowledge of the estimated full-field displacements and velocities data. Starting from the results of the augmented estimation, the following steps can be executed:

1. Extrapolation of velocity data $\dot{q}$ along the blade span by assuming a linear relation between the velocity and the position of the point:

$$\dot{q}(r)\hat{\imath}_2 = \Omega r, \qquad \dot{q}(r)\hat{\imath}_3 = \dot{\beta} r$$

2. Evaluation of the lift distribution along the blade span. Recalling Eq. (12), and given a certain flight condition with known pitch angle θ, the only unknown in the elemental lift will be the inflow angle ϕ or λ_i:

$$dL = dL(\lambda_i)$$

An iterative process can thus be executed by evaluating the inflow velocity from Eq. (18).
The results of the post-processing approach in terms of elemental lift distribution are shown in Fig. (15) and Fig. (16) for the two sensors layout in Table (2) and Table (3).

Presented at 46th European Rotorcraft Forum, Moscow, Russia, 8-11 September, 2020

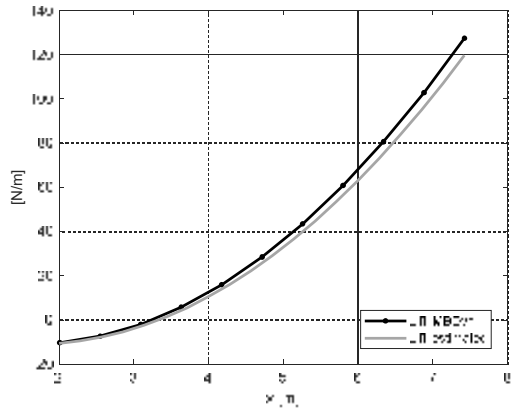

Figure 15. Elemental lift distribution along the blade span. Estimated values evaluated in post-processing. Sensors layout in Table (2).

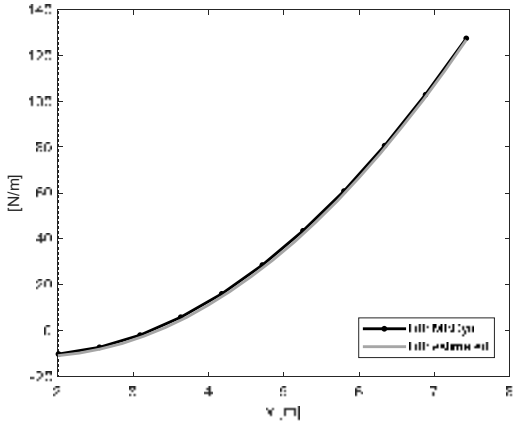

Figure 16. Elemental lift distribution along the blade span. Estimated values evaluated in post-processing. Sensors layout in Table (3).

Fig. (15) shows a mismatch between the reference lift and the estimated one, which increases going from the root to the tip, because of its sensitivity to the in-plane velocity. A good match is observed in Fig. (16) where the used estimated quantities are obtained from the sensors layout in Table (3). An advantage of this post-processing approach is not only to reach higher accuracy on the elemental aerodynamic force, but it also allows to reconstruct the full distribution along the blade span.

6. CONCLUSIONS

This contribution addresses the problem of states and load identification of a coupled multibody-aerodynamic helicopter blade model, recalling the approach proposed in [22]. A multibody articulated rotor with two blades is developed based on the finite segment theory, and a steady aerodynamic condition is considered with a uniform inflow model from the Blade Element Momentum Theory. The efficiency of the Kalman Filter estimation has been proven by using simulated reference data generated in MBDyn, an independent multibody simulation software. This means the inclusion of modelling errors in the estimation. Two advantages of the Kalman filtering technique allowed for the good performance on the results: i) usage of a reduced set of sensors which guarantee the observability of the system, or more specifically, of the estimated quantities; ii) when some modeling errors are present, e.g., structural properties or load location, all the uncertainties are compensated in the load estimation while still providing an accurate state reproduction. This is a great advantage of the Kalman Filter in the augmented formulation over other techniques cited in literature, reducing the need for highly accurate models, which are highly time-consuming to use, especially in the rotorcraft field. In the specific case of quasi-steady aerodynamic loads, the formulation of lift and drag is easily expressed in terms of the system states. Given a set of available sensor data, the approach proposed in [22] addressed the identification problem by considering the aerodynamic loads as external forces. The aim is to reach high accuracy only on states at position and velocity-level. This means that no aerodynamic evaluation is needed during the estimation and this is already an advantage as reduction of the computational cost. If a good accuracy on the estimated states can be obtained, an extrapolation of the velocity field data is allowed and the lift distribution presents only the dependence from the inflow velocity. An implicit function can be iteratively solved and the full lift distribution can be reconstructed in post-processing, showing an improvement with respect to the estimated forces. Future developments of the proposed methodology are the usage of feasible sensors, e.g., strain and accelerations, and to extend the proposed approach on a more complex system, as for example a flexible finite element blade model in order to allow for an experimental validation.

7. ACKNOWLEDGEMENTS

This research was funded by VLAIO (Flemish Innovation & Entrepreneurship) through its Baekeland Mandate project SINCRO (a general Strategy for load and parameter IdentificatioN for helicopter main Rotor system), n. HBC.2018.2086.

8. REFERENCES

[1] Haas, D. J.; Flitter, L.; Milano, J. Helicopter Flight Data Feature Extraction or Component Load Monitoring. J. Aircr. 1996, 33(1), 37-45.

[2] Ganguli, R.; Chopra. I.; Haas, D. J. Detection of helicopter rotor system simulated faults using neural

Presented at 46th European Rotorcraft Forum, Moscow, Russia, 8-11 September, 2020

networks. J. Am. Helicopter Soc. 1997, 42(2), 161–171.

[3] Ganguli, R.; Chopra. I.; Haas, D. J. Helicopter rotor system fault detection using physics based model and neural networks. AIAA J. 1998, 36(6), 1078–1086.

[4] Sarego, G.; Zaccariotto, M.; Galvanetto, U. Artificial neural networks for impact force reconstruction on composite plates and relevant uncertainty propagation. IEEE Aerosp. Electron. Syst. Mag. 2018, 33(8), 38-47.

[5] Ghajari, M.; Sharif-Khodaei, Z.; Aliabadi, M. H.; Apicella, A. Identification of impact force for smart composite stiffened panels. Smart Mater. Struct. 2013, 22(8), 085014.

[6] Bhatnagar, S.; Afshar, Y.; Pan, S.; Duraisamy, K.; Kaushik, S. Prediction of aerodynamic flow fields using convolutional neural networks. Comput. Mech. 2019, 64(2), 525-545.

[7] Bagherzadeh, S. A. Nonlinear aircraft system identification using artificial neural networks enhanced by empirical mode decomposition. Aerosp. Sci. Technol. 2018, 75, 155-171.

[8] Bernardini, G.; Porcelli, R.; Serafini, J.; Masarati, P. Rotor blade shape reconstruction from strain measurements. Aerosp. Sci. Technol., 2018, 79, 580-587.

[9] Serafini, J.; Bernardini, G.; Porcelli, R.; Masarati, P. In-Flight Health Monitoring of Helicopter Blades via Differential Analysis. Aerosp. Sci. Technol., 2019, 88, 436-443.

[10] Simon, D. Optimal state estimation: Kalman, H infinity, and nonlinear approaches. John Wiley & Sons: Hoboken, NJ, USA, 2006.

[11] Kalman, R. E. A new approach to linear filtering and prediction problems. J. Basic Eng. 1960, 82(1), 35-45.

[12] Xie, L.; Soh, Y. C.; de Souza, C. E. Robust Kalman Filtering for Uncertain Discrete-Time Systems. IEEE Trans. Autom. Controll 1994, 39(6), 1310-1314.

[13] Reza Moheimani, S. O.; Andrey V. Savkin; Ian R. Petersen. Robust Filtering, Prediction, Smoothing, and Observability of Uncertain Systems. IEEE Trans. Circuits and Syst. I Fundam. Theory Appl. 1998, 45(4), 446-457.

[14] Yang, G. H.; Wang, J. L. Robust Nonfragile Kalman Filtering for Uncertain Linear Systems with Estimators Gain Uncertainty. IEEE Trans. Autom. Control, 2001, 46(42), 343-348.

[15] Heredia, G.; Ollero, A. Sensor fault detection in small autonomous helicopters using observer/Kalman filter identification. In Proceedings of the IEEE International Conference on Mechatronics, Malaga, Spain, 14-17 April 2009, pp. 1-6

[16] Ebrahimian, H.; Astroza, R.; Conte, J. P.; Papadimitriou, C. Bayesian optimal estimation for output-only nonlinear system and damage identification of civil structures. Struct. Control Health Monit. 2018, 25(4), e2128.

[17] Van der Merwe, R. Sigma-Point Kalman Filters for Probabilistic Inference in Dynamic State-Space Models. PhD Dissertation, Oregon Health & Science University: Portland, Oregon, 2004.

[18] Azam, S. E.; Chatzi, E.; Papadimitriou, C. A dual Kalman filter approach for state estimation via output-only acceleration measurements. Mech. Syst. Signal Process. 2015, 60, 866-886.

[19] Cumbo, R., Tamarozzi, T., Janssens, K., & Desmet, W. (2019). Kalman-based load identification and full-field estimation analysis on industrial test case. *Mechanical Systems and Signal Processing*, *117*, 771-785.

[20] Risaliti, E., Tamarozzi, T., Vermaut, M., Cornelis, B., & Desmet, W. (2019). Multibody model based estimation of multiple loads and strain field on a vehicle suspension system. *Mechanical Systems and Signal Processing*, *123*, 1-25.

[21] Shabana, A. A. Dynamics of multibody systems. Cambridge university press, New York, USA, 2003.

[22] Cumbo, R.; Tamarozzi, T.; Jiranek, P.; Desmet, W.; Masarati, P. State and Force Estimation on a Rotating Helicopter Blade through a Kalman-Based Approach. MDPI, Sensors 2020, 20, 4196.

[23] https://www.mbdyn.org/

[24] Gessow, A. (1948). *Effect of Rotor-Blade Twist and Plan-Form Taper on Helicopter Hovering Performance.* NACA Technical Note 1542.

[25] Connelly, J. D., & Huston, R. L. (1994). The dynamics of flexible multibody systems: A finite segment approach—I. Theoretical aspects. *Computers & structures 50*(2).

[26] Naets, F.; Cuadrado, J.; Desmet, W. Stable force identification in structural dynamics using Kalman

Presented at 46th European Rotorcraft Forum, Moscow, Russia, 8-11 September, 2020

filtering and dummy-measurements. Mechanical Systems and Signal Processing, 2015, 50, 235-248.

[27] Huang, E. J. Computer aided analysis and optimization of mechanical system dynamics. Springer Science & Business Media: Berlin/Heidelberg, Germany, 2013.

[28] Gear, C. W.; Gupta, G. K.; Leimkuhler, B. J. Automatic integration of the Euler- Lagrange equations with constraints. J. Comput. Appl. Math, 1985, 12-13, 77-90.

[29] Connelly, J. D.; Huston, R. L. The dynamics of flexible multibody systems: A finite segment approach—I. Theoretical aspects. Computers & structures, 1994, 50(2), 255-258.

[30] Ascher, U. M.; Petzold, L. R. Computer methods for ordinary differential equations and differential-algebraic equations. Siam 1998, 61.

[31] Leishman, G. J. Principles of helicopter aerodynamics. Cambridge university press: New York, USA, 2006.

[32] Przemieniecki, J. S.; Przemieniecki. Theory of matrix structural analysis - Vol. 1. Courier Corporation: New York,
USA, 1968.

[33] Ghiringhelli, G. L.; Masarati, P.; Mantegazza, P. Multibody implementation of finite volume C beams. AIAA J.l 2000, 38(1), 131-138.

Presented at 46th European Rotorcraft Forum, Moscow, Russia, 8-11 September, 2020